Ballistic Re-entry Vehicle Dispersion Due to Precession Stoppage

T. C. Lin* and W. R. Grabowsky†
TRW Electronics and Defense Sector, San Bernardino, California
K. E. Yelmgren‡
Ballistic Missile Office, Norton AFB, California
and
M. Landa*
Aerospace Corporation, El Segundo, California

Ballistic re-entry vehicle (RV) precession stoppage phenomenon is investigated analytically and several postulated reasons for its occurrence are discussed. Both analytical solutions and six-degree-of-freedom (6DOF) simulations are presented. In addition to the familiar phenomena of roll through zero (RTZ), roll near zero (RNZ) and angle-of-attack divergence, there are four additional aerodynamic forcing functions that are found to be particularly interesting and significant since they can induce the so-called "space-fixed-trim" phenomenon i.e., the lift vector becomes momentarily stationary in space. These four forcing functions are: a) a shift from body-fixed to wind-fixed trim moment in high q_∞ environments; b) RV with transient unstable aerodynamic stability derivative; c) trim plane migrations induced by a series of asymmetric nose spallations; and d) a Magnus-type out-of-plane moment in conjunction with the wind-fixed moment induced by ablation lag phenomena. When this occurs, the trajectory deflection becomes prohibitively large. According to the present analytical/numerical results, the initial spin rate can be crucial for the magnitude as well as the direction of the RV dispersion. Finally, some possible physical mechanisms which would cause RV precession stoppage are suggested.

Nomenclature

A = RV reference area
C_A = axial force coefficient
C' = constant defined in Eq. (12)
C_ℓ, C_m, C_n = roll, pitch, and yaw moment coefficients, respectively
$C_{m_{\text{body}}}, C_{m_{\text{wind}}}$ = body-fixed and wind-fixed pitch moment coefficients
$C_{m_q} + C_{m_{\dot\alpha}}$ = pitch damping coefficient
$C_{\ell_p}, C_{\ell_\beta}$ = roll damping derivatives
C_N = normal force coefficient
$C_{N_\alpha}, C_{L_\alpha}$ = normal force/lift force derivative
$C_{n_{\alpha p}}$ = $\partial^2 C_n / \partial\alpha \partial p$
C_{y0}, C_{z_0} = lateral force coefficients caused by aerodynamic asymmetries in y-body/z-body direction
d = RV base diameter
h = altitude
I = RV pitch or yaw moment inertia
I_x = roll moment inertia
J = trajectory deflection angle
k = radius of gyration
L = RV length
m = RV mass
p = RV roll rate
$\dot p$ = dp/dt
P_{cr} = critical roll rate = $\omega/\sqrt{1-\mu^2}$
q_∞ = freestream dynamic pressure
$\bar S$ = $y + iz$ = helix radius
$\ddot s$ = $d^2 s/dt^2$
SM = static margin, $(X_{cp} - X_{cg})/L$
t = time
W = RV weight
X, Y, Z = distance along the inertia frame, X along the mean flight path
α, β = pitch and yaw angle-of-attack
α_T = trim angle-of-attack
$\Delta\alpha_T$ = step trim
ΔV = RV lateral velocity perturbation
ϵ = RV cg offset
ζ = damping parameter, see Eq. (5)
ζ_T = $\beta + i\alpha$ = complex total angle-of-attack
μ = I_x/I
$\dot\psi$ = precession rate
ψ, θ, ϕ = Euler angles
ω = natural pitch frequency $[-C_{m_\alpha} q_\infty A d I^{-1}]^{1/2}$
$(\dot{})$ = $d(\ )/dt$

Presented as Paper 82-1307 at the AIAA 9th Atmospheric Flight Mechanics Conference, San Diego, Calif., Aug. 9-11, 1982; submitted Jan. 31, 1983; revision received Aug. 31, 1983.

*Section Head. Member AIAA.
†Department Head, Aeromechanics and Propulsion. Member AIAA.
‡Major, USAF. Member AIAA.

I. Introduction

THE dispersion of a ballistic RV is generally small as a result of a helix precession motion which results in a lift-averaging process. Usually an initial spin is imposed on the RV after separation from the booster/bus, and on re-entry the subsequent gyroscopic motion when combined with the aerodynamic forces makes the RV revolve into a helical motion. However, even with this rolling/precession motion, there may still exist a lift vector nonaveraging phenomenon, i.e., rapid variations in the magnitude/orientation of the lift vector or the roll rates.[1-4] The objective of this paper is to identify possible aerodynamic forcing functions and their corresponding physical phenomena that would induce pre-

cession slowdown and hence large RV dispersion. An approximate analytical formulation with closed form solutions is developed in Section II. From these simple solutions, seven possible causes of precession stoppage are identified and discussed in Section III. Two of the more interesting forcing functions were checked with 6DOF simulations. The results are presented in Section IV. The physical mechanism that would result in the aerodynamic forcing functions causing precession stoppage are summarized in Section V.

II. Analysis

The dispersion of the RV can be analyzed by considering the following differential equations, which describe the lateral motions of the RV c.g. about the mean flight path[5] for small total angle-of-attack* (see Fig. 1a):

$$\ddot{\bar{S}}=\ddot{Y}+i\ddot{Z}=\frac{q_\infty A}{m}\left\{\left[C_{y_0}+iC_{z_0}\right]e^{i\phi}+i\left[C_A-C_{N_\alpha}|\zeta_T|\right\}e^{i\int\dot{\psi}dt}$$

$$\ddot{X}=\frac{q_\infty A}{m}\left[C_A+C_{N_\alpha}|\zeta_T|^2-C_{y_0}\beta-_{z_0}\alpha\right] \quad (1)$$

For a slender RV with small aerodynamic asymmetries, Eq. (1) can be simplified to:

$$\ddot{\bar{S}}=-\frac{q_\infty Ai}{m}C_{L_\alpha}|\zeta_T|e^{i\int\dot{\psi}dt} \quad (2)$$

Then the corresponding trajectory deflection, ΔJ, due to lift nonaveraging, can be estimated with the following relation:

$$\Delta J=|\Delta V|/V_\infty=\text{trajectory deflection angle}$$

and

$$\Delta\dot{\bar{V}}=\dot{Y}+i\dot{Z}=-\frac{iA}{m}\int_0^t C_{L_\alpha}|\zeta_T|q_\infty e^{i\int\dot{\psi}dt}dt \quad (3)$$

It is known that the impact miss dispersion is a statistical parameter with randomness entering through the lift amplitude $C_{L_\alpha}|\zeta_T|$ and phase $\text{Exp}(i\dot{\psi}t)$. However, for illustrative purposes, a quasisteady solution of Eq. (3) can be obtained for small time intervals (such that the aero coefficients are almost constant), and is given as:

$$\bar{S}\doteq\bar{C}_1+\bar{C}_2t+\frac{q_\infty AC_{L_\alpha}i}{m\dot{\psi}^2}|\bar{\zeta}_T|e^{i\int\dot{\psi}dt}=Y+iZ \quad (4)$$

Here $\bar{C}_1$ and $\bar{C}_2$ are arbitrary constants which are determined by initial conditions at the start of each interval. A rapid change in any of the parameters (e.g., due to frustum boundary layer transition appearing in Eq. (3) would have the effect of producing a non-zero value of $\bar{C}_2$ for the subsequent time interval, and thereby produce a trajectory dispersion. When $\bar{C}_1=\bar{C}_2=0$, Eq. (4) essentially states that the centrifugal force resulting from the vehicle's helix motion is equal to and opposite to the lateral trim forces. The helix radius produces a miss distance at impact which increases with increasing values of q_∞, C_L and becomes excessively large as $\dot{\psi}\to 0$. For example, a 300-lb RV with base radius $r_b=1$ ft, $\gamma=30°$, $\dot{\psi}=1$ cps, $C_{L_\alpha}=1.2$, $q_\infty=10^5$ lb/ft^2, and $|\bar{\zeta}_T|=1°$, the miss distance is approximately 18 ft cross-range and 36 ft down-range. The impact miss due to the helix motion is, in most investigations, not included in the dispersion budget.

The missile motion is described in terms of the Euler angle coordination, ψ, θ, ϕ, and the moment equations of motion can be written as (see Fig. 1b):

$$I\ddot{\theta}+I_xp\dot{\psi}\sin\theta-I\dot{\psi}^2\sin\theta\cos\theta+2I\zeta\omega\dot{\theta}=C_mq_\infty Ad+\left[C_{m_{\text{body}}}\cos\phi+C_A\epsilon\sin\phi/d\right]q_\infty Ad \quad (5a)$$

$$I\frac{d}{dt}\left[\dot{\psi}\sin^2\theta\right]-I_xp\sin\theta\dot{\theta}+2\zeta\omega\dot{\psi}\theta^2I=C_nq_\infty Ad\sin\theta+\left[C_{m_{\text{body}}}\sin\phi-C_A\epsilon\cos\phi/d\right]q_\infty Ad\sin\theta \quad (5b)$$

$$I_x\dot{p}=C_\ell q_\infty Ad+C_{\ell_p}\frac{pd}{2V_\infty}q_\infty Ad+C_N\epsilon q_\infty A\cos\phi+C_{\ell_\beta}\theta\sin\phi q_\infty Ad \quad (5c)$$

$$p=\dot{\phi}+\dot{\psi}\cos\theta \quad (5d)$$

where

$$\zeta=\frac{1}{2m}\left(\frac{\rho AI}{(2C_{N_\alpha}\bar{A}\bar{M}\cdot L}\right)^{1/2}\left[C_{N_\alpha}-\left(C_{m_q}+C_{m_{\dot{\alpha}}}\right)d^2/2k^2\right]$$

III. Precession Stoppage Causes

Equation (4) shows that a large RV trajectory deflection occurs during re-entry when $\dot{\psi}\to 0$. Equation (5) shows that this would happen under several situations. These situations are as follows:

Roll-Through-Zero (RTZ)

When an RV is in lunar motion, i.e., $\dot{\phi}=0$, then "roll-through-zero" implies precession stoppage because $p=\dot{\phi}+\dot{\psi}$

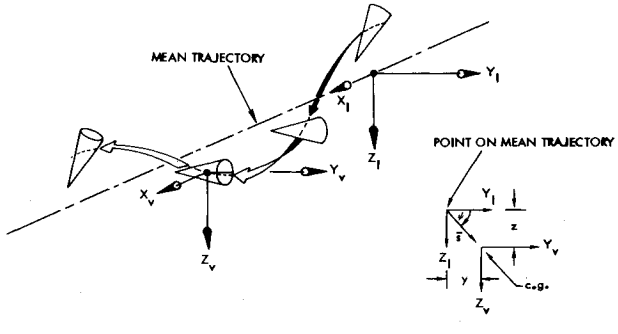

Fig. 1a Motion of the c.g. about the mean flight path.

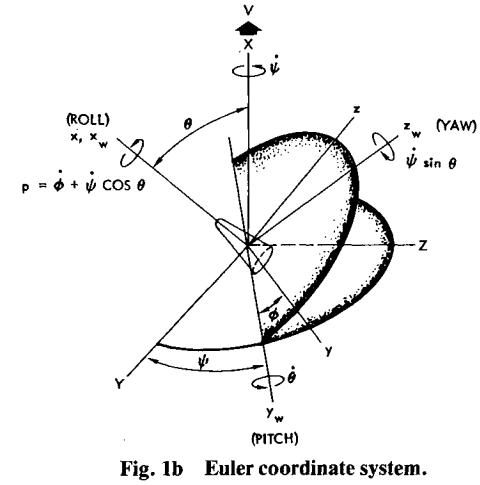

Fig. 1b Euler coordinate system.

cos $\alpha \simeq \psi = 0$, for small α. It must be emphasized that the necessary condition for $\dot{\psi}=0$ when $p=0$ is $\dot{\phi}=0$. Usually this condition occurs momentarily when a slightly asymmetric missile in rolling trimmed flight has a roll-rate reversal of a roll torque in direction opposite to p. The cross-range dispersion resulting from a roll-through-zero can be approximately estimated as[12]:

$$\bar{S} = -\sqrt{\frac{\pi}{2}}\, g(\rho_\infty V_\infty h)_{p=0} \left\{ \sin \gamma_{p=0} \left[\frac{W}{C_{L_\alpha} \alpha A} \right] |\dot{p}|^{1/2} \right\}$$

Relatively Large Increase in Angle-of-Attack[1]

If an initially untrimmed RV is subject to a static in-plane moment that has a trim angle θ_p, i.e.,

$$M_p = C_m q_\infty A d = I\omega^2 \theta_p$$

and the other aerodynamic forcing functions appearing in the Euler angle coordinate moment equations [i.e., Eq. (5) assumes the special case

$$\epsilon = C_{m_b} = C_n = C_{m\dot{\psi}} = 0;$$

then integration of the governing equations yields (for $\theta << 1$):

$$(1 - \dot{\psi}^2/\omega^2)\theta = \theta_p, \tag{6a}$$

$$\left(\dot{\psi} - \frac{\mu p}{2}\right)\theta^2 = \text{constant} \neq 0$$

or

$$\dot{\psi}\theta^2 = \dot{\psi}_0 \theta_0^2 = \text{constant for} \frac{\mu p}{2} << \dot{\psi} \tag{6b}$$

The subscript "0" corresponds to the initial conditions at $t=0$. For a relatively large increase in angle-of-attack due to in-plane disturbances, Equation (6b) yields $\dot{\psi}/\dot{\psi}_0 \sim (\theta_0/\theta)^2 << 1$. Note that Eq. (6b) does not mean $\dot{\psi}=0$, but rather implies $\dot{\psi} \to 0$. The RV dispersion can also become excessively large when $\dot{\psi}$ is small but nonzero. This is the well known case of precession near zero or roll near zero if the RV is in lunar motion. For instance the lateral induced velocity of a trimmed missile (i.e., $\dot{\phi}=0$, $p=\dot{\psi}$) can be approximated as[1]:

$$\Delta V = \frac{i \Delta L}{m\dot{\psi}} (1 - p^2/p_{cr}^2)$$

where ΔL = step trim force due to a body fixed disturbance

$$= C_{N_\alpha}(\Delta\alpha_T) q_\infty A$$

$$\Delta\alpha_T = \text{step trim}$$

Typically, the lift nonaveraging dispersion can be large, e.g., $\Delta V \doteqdot 91.4$ m/s when $m=113.4$ kgs, $p=120$ deg/s, $q_\infty = 73.236$ kg/cm^2, $p/p_{cr} << 1$, $C_{N_\alpha}=1.2$, $\Delta\alpha_T = 0.5$ deg and $r_b = 0.3048$ m.

The Appearance of Small Impulsive Out-of-Plane Moment[1] Coupled with an In-Plane Trim Moment

When the yaw moment assumes a special form, i.e.,

$$C_n = -I\theta\dot{\psi}_0 \delta(t)/q_\infty A d$$

where $\delta(t)$ = Dirac-Delta function and if $\epsilon = C_{m_b} = 0$ and $C_m = -C_{m_\alpha}(\theta - \theta_p)$ simultaneously, Platus[1] has shown that the precession rate will decrease to and remain zero, i.e., $\dot{\psi}=0$. Therefore, a small impulsive out-of-plane moment, coupled with in-plane moment perturbation, can drive the precession rate to zero for arbitrary initial conditions. In practical applications one can approximate the $\delta(t)$ by a rectangular pulse of duration t_p and magnitude of $-I\theta\dot{\psi}_0/q_\infty A dt_p$. Then this would cause a transverse velocity perturbation,[1]

$$\Delta V = C_{L_\alpha} \theta_p q_\infty A t_p / m$$

Transient Unstable or Neutral Stability Derivative (i.e., $C_{m_\alpha} \geq 0$ or $\omega = 0$).

Under the approximations of quasisteady condition ($\ddot{\theta} = \dot{\theta} = 0$), negligible damping ($\zeta = 0$) and $\epsilon\, C_{m_b} = 0$, the Euler angle equations (i.e., Eq. 5a) would be simplified to:

$$(\omega^2 + \mu p\dot{\psi} - \dot{\psi}2)\theta = 0 \tag{7}$$

For $\theta \neq 0$, one solution to Eq. (7) is $\omega = \dot{\psi} = 0$, if $C_{m_\alpha} = 0$. One well known example for unstable C_m is the pitching moment observed on a blunt face cylinder (see Fig. 2). It is noted C_m assumes zero value at $\alpha = 0$, 21.8, 31, and 83 deg, however, the stable trim points only exist at $\alpha = 21.8$ and 83 deg. Then if the missile angle-of-attack oscillation about the trim point (i.e., $\alpha = 21.8$ deg) is large enough, α may cross into the range where $C_{m_\alpha} \geq 0$. Under these conditions the precession rate would slow down, at least momentarily.

A Shift from Body-Fixed to Wind-Fixed Trim Moment in a High q_∞ Environment

The precession motion of an RV at high altitude (i.e., $q_\infty << 1$) is initiated by the initial spin and original angle-of-attack. At low altitude, a body fixed disturbance (e.g., nose tip asymmetric ablation) and the yaw moment (C_n) could be a

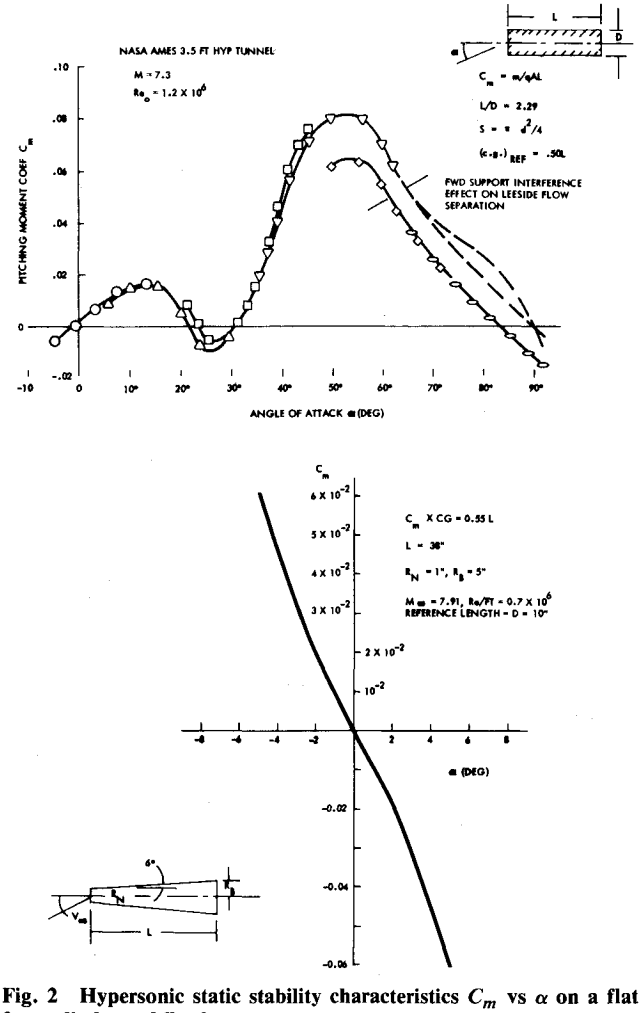

Fig. 2 Hypersonic static stability characteristics C_m vs α on a flat face cylinder and flat face core.

driver modifying the precession motion. For the special case of sudden disappearance of C_{m_b} and C_n in a high q_∞ environment, the precession equation [Eq. (5b)] becomes:

$$\frac{d}{dt}(\dot{\psi}\theta^2) = -2\zeta\omega(\dot{\psi}\theta^2),\ t \geq t_0 \tag{8}$$

Other assumptions implied in Eq. (8) are $\theta << 1$, $\mu p\theta\dot{\theta} << 1$ and $\epsilon = 0$. Equation (8) can then be integrated as:

$$\theta^2\dot{\psi} = (\theta^2\dot{\psi})_0 \exp[-\Lambda(t-t_0)],\ t \geq t_0 \tag{9}$$

where $\Lambda = \left[\frac{C_{N_\alpha} q_\infty AI}{mV_\infty} - (C_{m_q} + C_{m_{\dot{\alpha}}}) q_\infty A d^2/2V_\infty\right]/I = 2\zeta\omega$

Furthermore, under the assumptions of quasisteady condition, and the in-plane pitch moment having the following form

$$C_m = C_{m_\alpha}(\theta - \theta_{\text{trim}})$$

Using this, the angle-of-attack equation can then be integrated to give:

$$[\omega^2 + \dot{\psi}(\mu p - \dot{\psi})]\,\theta = \omega^2\theta_{\text{trim}} \tag{10}$$

The steady-state solution to Eq. (10), which is relevant to our problem, is

$$\theta = \theta_{\text{trim}}$$

which results if

$$\dot{\psi} = \mu p \quad \text{or} \quad \dot{\psi} = 0$$

Equations (9) and (10) indicate an exponential decay of the precession rate after the disappearance of C_{m_b}. When the damping parameter $\Lambda = 0(1)$ or $\Lambda >> 1$, the RV precession rate, $\dot{\psi}$, will rapidly decrease to an almost zero, and large missile dispersion will result. It should be noted that the mechanism (2) mentioned above, i.e., Eq. (6b), is a special case of Eq. (9) for $\Lambda = 0$. However, the precession slowdown considered here does not require $\theta_p/\theta >> 1$; rather $\dot{\psi}$ is exponentially damped out due to the inherent pitch and normal force damping under the high freestream dynamic pressure, q_∞ environment.

It should be emphasized that the case of interest (i.e., RV at low altitude where the freestream dynamic pressure is high) usually involves body-fixed disturbances. For the occurrence of RV precession stoppage, the body-fixed trim must disappear concurrently with the advent of the wind-fixed trim. However, the precession stoppage would occur even if no body-fixed trim is present initially. The real cause of the precession stoppage is the appearance of the wind-fixed trim moment, which in the absence of the body-fixed trim and with the inherent normal force damping at high q_∞ environment, produces the conditions $\dot{\psi} \to 0$ and $\dot{\phi} \to p$.

Trim Plane Migrations Induced by Sequences of Asymmetric Nose Spallation

The trim meridian may undergo rapid changes as a result of a series of different asymmetric nose tip shapes that would be produced if the nose rapidly erodes in high pressure environments. A special case of interest corresponds to the windward meridian migration rate equal to RV roll rate. This situation implies that $\dot{\psi} \to 0$, since Eq. (5d) indicates $\dot{\psi} = p - \dot{\phi}$ as $\dot{\phi} \approx p$. This mechanism is suggested by the observation of ballistics range erosion data on nosetip shape change. Thyson, et al.,[1] found that the nose tip erosion process *cannot* always be viewed in terms of the axial translation of a smooth, symmetric, blunt configuration. Frequently, nose shape irregularities such as shoulder asymmetry and Z-rod matrix projections have been observed during tests. This continuous development of the erosive shape irregularities is postulated to be the basic mechanism responsible for trim plane migrations.

Out-of-Plane Moment Induced by Ablation Time-Lag with Wind-Fixed Trim Moment

When an out-of-plane moment is induced and assumes a form similar to Magnus moment, i.e.,

$$C_n = -C_{n_{\alpha p}}\dot{\psi}\theta \tag{11a}$$

and the pitch plane moment is:

$$C_m = -C_{m_\alpha}(\theta - \theta_p) \tag{11b}$$

Then the basic equations [i.e., Eq. (5)] can be integrated to give (with $\epsilon = C_{m_{\text{body}}} = 0$):

$$(1 - \dot{\psi}^2/\omega^2)\theta = \theta_p \approx \text{constant} \to \theta \approx \theta_p = \text{constant} = \theta_0$$

and

$$\dot{\psi}\theta^2 = (\dot{\psi}\theta^2)_0 \exp[-\lambda t] \tag{11c}$$

or

$$\dot{\psi} = \dot{\psi}_0 \exp[-\lambda t]$$

Table 1 Sphere-cone($\theta_c = 6°$, $R_N/R_b = 0.15$) aerodynamics

α (Degree)	C_N	C_A	$-C_m$
0	0	0.048	0
1	0.021	0.048	0.0162
3	0.077	0.049	0.0594
5	0.145	0.051	0.11194
7.5	0.23		0.1774
10	0.315		0.243
15	0.485		0.3741
20	0.655		0.509
90	3.305		2.5495

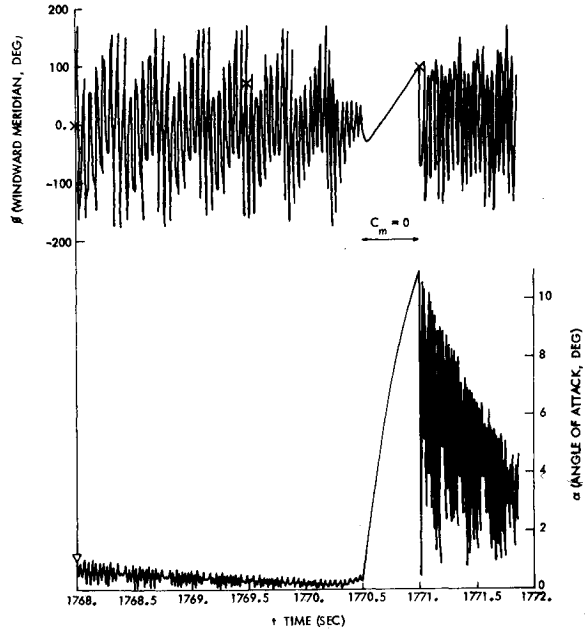

Fig. 3 6DOF simulation results for transient $C_{m_\alpha} = 0$(ϕ and α vs time).

where $\lambda = 2\zeta\omega \pm |C_{n_{\alpha p}}| q_\infty Ad/I = 2\zeta\omega \pm \kappa$

$$\kappa = |C_{n_{\alpha p}}| q_\infty Ad/I$$

When $\kappa < 2\zeta\omega$, then $\lambda > 0$, and an exponential decay of the precession rate is predicted and the effect of the out-of-plane moment is to enhance the effective damping of the precession. For $\kappa > 2\zeta\omega$, an amplification of $\dot{\psi}$ may occur. Normally Eq. (11c) is used to explain the angle-of-attack divergence observed on re-entry flight when $2\zeta\omega \pm \kappa < 0$ and $\dot{\psi} \approx$ constant.[13] When $\lambda < 0$, Eq. (11c) suggests $\theta^2 = \theta_0{}^2 \exp(-\lambda t)$, i.e., angle-of-attack divergence.

It follows shat this mechanism or Waterfall's[6] ablation time-lag postulation can be used to interpret the precession stoppage phenomena when the freestream dynamic pressure is not high. Since both the magnitude and the algebraic sign of $Cn_{\alpha p}$ are important in predicting the amplification factor (i.e., λ), it appears that the spin rate of the RV and the heatshield material properties play an important role in estimating dynamic instability phenomena. It should be noted that Platus' impulsive C_n, discussed previously, is similar to the Magnus moment given in Eq. (11a).

The precession stoppage causes of (2), (3), (5) and (7) all require the application of a predominantly in-plane wind-fixed trim moment, which is the primary cause of the precession stoppage. The difference between causes (5) and (7) is the presence of a small out-of-plane moment, which enhances the dampings of the precession motion, where the inherent aerodynamic pitch and normal force damping is low, e.g. at high altitude. The distinction between mechanisms (2) and (5) is that the latter does not require a relatively large increase in angle-of-attack [i.e., $\theta >> \theta_0$, see Eq. (6b)].

IV. Six-Degree-of-Freedom Simulation

The mechanisms discussed above would result in $\dot{\psi} \to 0$, provided that the many restrictive assumptions are valid. These analytical results will now be examined with a full 6DOF simulation. The input mass properties and the aerodynamic coefficients are as follows:

$I_x = 1199.8$ kg-cm^2

$I_y = 27800.7$ kg-cm^2

$A =$ base area $= 0.0511$ m^2

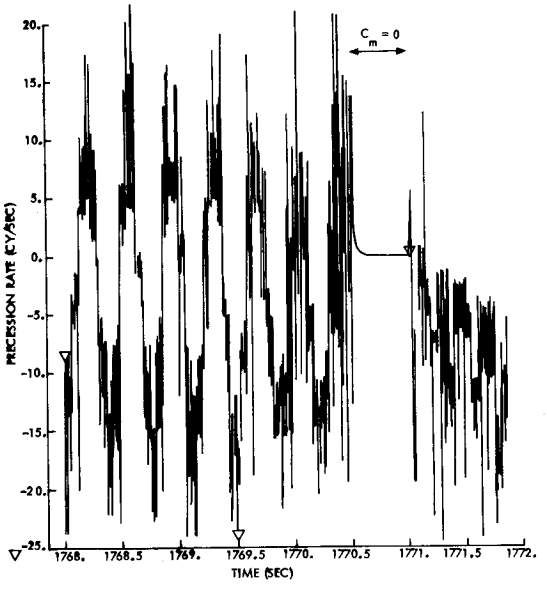

Fig. 4 6DOF simulation results for transient $C_{m_\alpha} = 0 (\dot{\psi}$ vs $t)$.

$\theta_c = 6°$, weight $= 40.82$ kg

$\epsilon =$ c.g. offset $= 0.01016$ cm

The calculations were initiated at $h = 18.29$ km with $V_\infty = 6.51$ km/s. The RV roll rate is kept at a constant value, i.e., $p = p_0$ and $C_{\ell_0} = C_{\ell_p} = 0$ [see Eq. (5c)].

The first three mechanisms mentioned in Section III have been extensively studied by several investigators[1] and consequently are not examined in this 6DOF simulation.

RV with Transient Unstable or Neutral C_m

The input pitch moments are given below and we will impose $C_m = C_{m_\alpha} = 0$ for 0.5 s (i.e., from $t = 1770.5$ s to $t = 1771$ s, see Fig. 3).

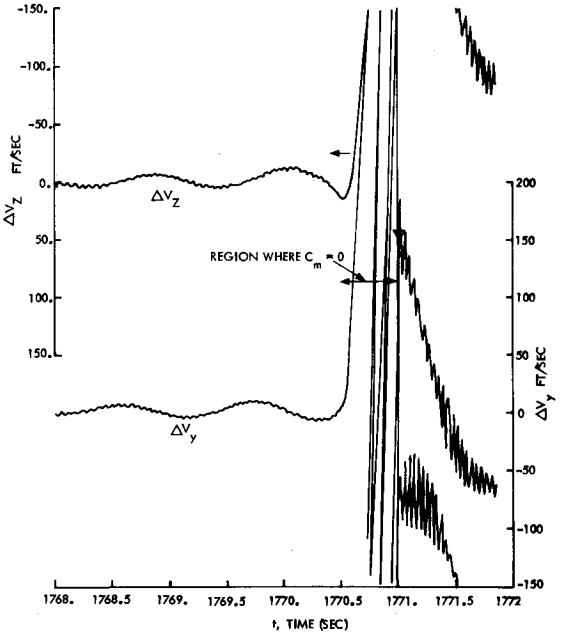

Fig. 5 6DOF simulation results for transient $C_{m_\alpha} = 0 (\Delta V$ vs $t)$.

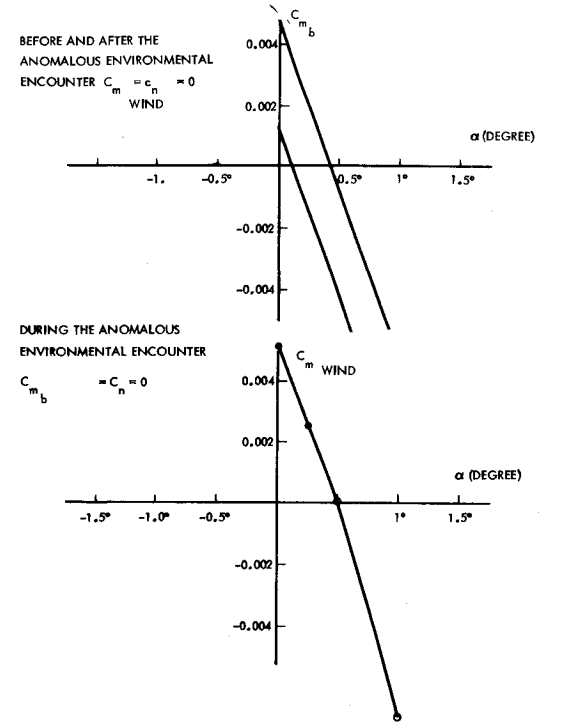

Fig. 6 Input aerodynamic pitching moment coefficients.

$$C_{m_b} = -0.01(\alpha - 0.3°), t < 1770.5, t > 1771 \text{ s}$$

$$C_{m_b} = 0,\ C_{m_\alpha} = 0 = C_m,\ 1770.5 \le t \le 1771 \text{ s}$$

The numerical results for both the angle-of-attack and the windward meridian are illustrated in Fig. 3. The precession rate history is depicted in Fig. 4. As expected, when the input C_{m_α} assumes a zero (or positive C_{m_α}) value, α starts to increase rapidly. Simultaneously, the precession rate decreases to zero value within 0.14 s after we impose $C_{m_\alpha} = 0$, and ϕ would more or less follow the roll rate [see Eq. (7)]. The total lateral induced velocity also becomes very large as shown in Fig. 5. Since the angle-of-attack increases so drastically, the RV may not survive because of structural failure, in which case the error caused by the precession slowdown becomes a secondary issue. Therefore, in most cases, this phenomenon would be important for dispersion considerations only when the forcing function (i.e., $C_m \ge 0$) appears for a short duration as a transient phenomena.

A Shift from Body-Fixed to Wind-Fixed Trim Moment in High q_∞ Environment

The second case considered here for 6DOF simulation is the fifth mechanism mentioned previously in Section III. The aerodynamic forcing function is given in Fig. 6, which shows the input moment is switching from C_{m_b} to $C_{m_{\text{wind}}}$ for a 1 s duration, i.e.,

—Before and after the anomalous aerodynamic forcing function

$$C_n = 0$$

$$C_{m_b} = -0.011\,(\alpha - \alpha_T)$$

α_T = trim angle which assumes to increase linearly from 0.1° to 0.4° in 0.5 s (starting at t = 1770 s)

—During the anomalous environmental encounter

$$C_{m_b} = 0,\ C_n = 0$$

$$C_{m_{\text{wind}}} = -0.01\,(\alpha - 0.5°)$$

The numerical results for the precession rate is depicted in Fig. 7 for the case of roll rate $p = p_0 = 310$ deg/s. As soon as the external moment is switched from body-fixed to wind-fixed, the precession rate starts to decrease. It drops to $\dot{\psi}(0)/e (e = 2.71828)$ within 0.4 s which is comparable to the time constant given in Eq. (6a) i.e.,

$$\frac{I}{\Lambda} = \left[\frac{C_{N_\alpha} q_\infty A}{mV_\infty} - (C_{m_q} + C_{m_{\dot{\alpha}}}) q_\infty A d^2/2V_\infty I\right]^{-1} \doteqdot 0.37 \text{ s}$$

$$q_\infty = 61.03 \text{ kg/cm}^2$$

$$V = 5791.2 \text{ m/s}$$

$$C_{N_\alpha} = 2/\text{ radian}$$

$$C_{m_q} + C_{m_{\dot{\alpha}}} = -0.01^{\S}$$

The lateral perturbation velocity [i.e. Eq. (3)] is shown in Fig. 8, which indicates that the large ΔV appears soon after the disappearance of C_{m_b}. Figures 9 and 10 illustrate the lateral forces and moments as observed by the onboard sensors (i.e., accelerometer and gyro). As can be seen, these two signatures did not indicate any abnormal RV dynamics. The windward meridian and angle-of-attack are given in Fig. 11 and show ϕ is almost rotating at the RV spin rate (i.e., $\dot{\phi} \approx p$).

When the roll rate $p = -310$ deg/s instead of 310 deg/s, the 6DOF simulation result for $\dot{\psi}$ is given in Fig. 12, which shows

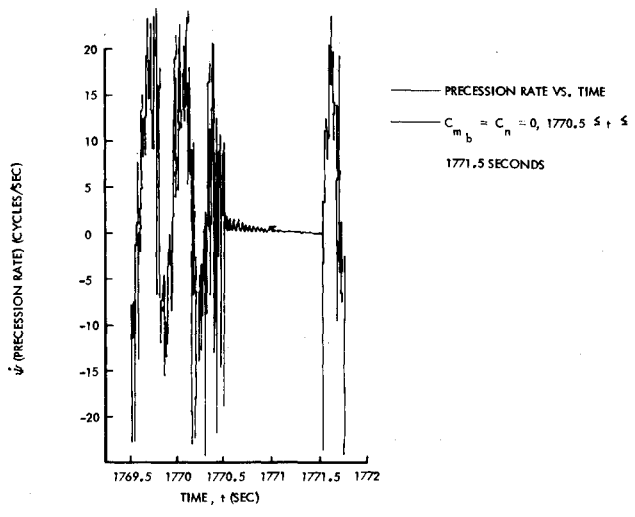

Fig. 7 6DOF simulation results ($p = 310$ deg/s)—precession rate vs time—$C_{m_b} = C_n = 0$, $1770.5 \le t \le 1771.5$ s.

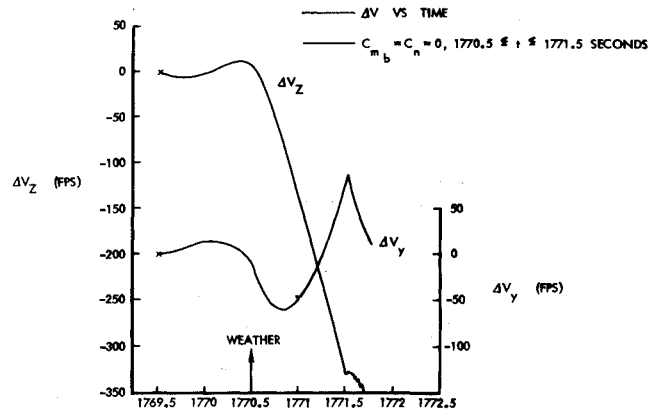

Fig. 8 6DOF simulation results ($p_0 = 310$ deg/s)—ΔV vs time—$C_{m_b} = C_n = 0$, $1770.5 \le t \le 1771.5$ s.

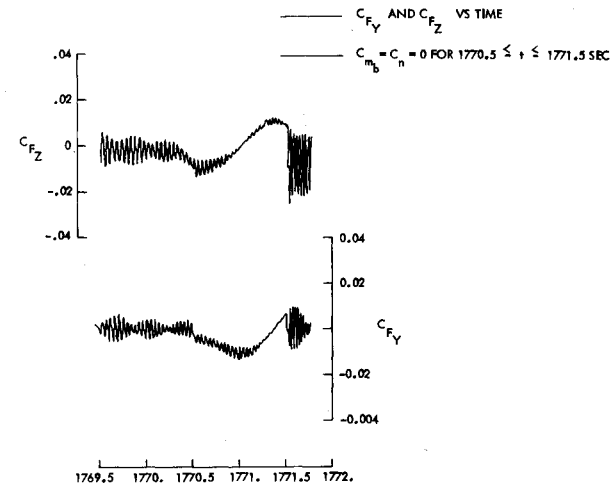

Fig. 9 6DOF simulation results ($p_0 = 310$ deg/s)—C_{F_Y} and C_{F_Z} vs time—$C_{m_b} = C_n = 0$, $1770.5 \le t \le 1771.5$ s.

§A more realistic value for the pitching damping derivative would be $C_{m_q} + C_{m_{\dot{\alpha}}} = -1.5$. When using this value, it yields $1/\Lambda \doteqdot 0.25$ s.

that the precession rate also slows down after the external moment switches from C_{m_b} to $C_{m_{\text{wind}}}$. The time constant Λ^{-1} is still about 0.4 s. Similarly, we observed that ΔV increases dramatically (see Fig. 13), but is of *opposite* sign when compared with the case of $p=310$ deg/s (see Fig. 8). This is an interesting as well as significant result, since it indicates that the RV would disperse to the left side of the unperturbed trajectory when $p>0$ and to the right side when $p<0$.

Finally, we consider a case where the roll rate is $p=930$ deg/s. The 6DOF calculated results suggest that the precession rate also begins to decrease after the external moment switches from C_{m_b} to $C_{m_{\text{wind}}}$ (see Fig. 14); however, now the ΔV is smaller (see Fig. 15) than the case when $p=310$ deg/s. This reduction is ΔV is probably due to the following reasons: the initial precession rate, $\dot{\psi}(0)$, at the time of the disappearance of C_{m_b} is much larger for the case of $p=930$ deg/s [e.g., see Eq. (9)] and the term $I_x p\theta\dot{\theta}/I$ appearing in the precession equation [see Eq. (5b)] is larger for $p=930$ deg/s case.

In summary, the 6DOF simulation results suggest that the transient unstable C_{m_α}, as well as the disappearance of the body-fixed moment coupled with the introduction of a wind-fixed moment, would result in an exponential decay in $\dot{\psi}$. These 6DOF numerical results are similar to the simple analytical results given in Eq. (7) and (9). Obviously, the rapid decrease of $\dot{\psi}$ is not a desirable situation for a ballistic RV when the ambient dynamic pressure is high. The numerical results also indicate first, that the precession rate slow-down depends strongly on the initial RV roll rate, and second, that the direction of RV spinning may determine the RV dispersion direction, e.g., a clockwise rotation, RV trajectory deflects to the left, and a counterclockwise to the right.¶ Another subtle, but important observation is that the precession stoppage phenomena does not seem to be strongly affected by the magnitude of the RV static margin.

V. Physical Mechanism

From the mathematic relations, we have identified several forcing functions which would result in RV precession stoppage. Physical mechanisms that may reproduce those mentioned force/moments are summarized below.

Roll-Through-Zero (RTZ)

RTZ can result from negative RV frustum/nose roll torque on missiles with trim/c.g.-offset coupling or from an RV with a principle axis tilt. These undesirable motions have been observed on many flight experiments. It is essential to avoid RTZ, particularly when the missile is in lunar motion. This can be achieved by careful design of the aerodynamic configuration of the RV and by designing the structure and heatshield to avoid mass and ablation asymmetries.

Unstable C_m

Slender missiles with unstable (or neutral) static stability derivatives have been found on flat face cylinders (see Fig. 2). However, wind tunnel measurements on flat face 6° cone ($R_N/R_b=25\%$) indicates C_{m_α} is stable for angle-of-attack $-8°\le\alpha\le 8°$ (see Fig. 2). The wind tunnel conditions corresponds to $M_\infty=8$, Re/meter $=1.1\times10^6$.

The RV aerodynamics during the frustum boundary layer transitions have been extensively investigated. Some researchers suggest that C_{m_α} can become momentarily unstable due to asymmetric boundary layer transition patterns which causes temporary angle-of-attack divergence.

Another postulated mechanism for unstable C_m is when the RV travels through a highly erosive environment, e.g., an unusually high stagnation heating ($\sim 100\text{kW/cm}^2$) such as NASA Galileo Probe.[15] The frustum/nose tip spallations could eject debris into the shock layer. Hence, the flowfields are significantly perturbed (see Fig. 16). The resulting two-phase flow patterns have been observed in both wind tunnel as well as ballistic range tests. Under certain circumstances,

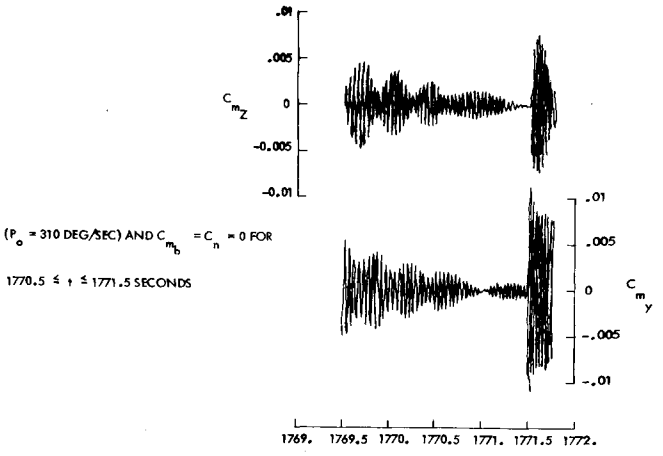

Fig. 10 6DOF simulation results C_{m_Y} and C_{m_Z} vs $t(p_0=310$ deg/s) and $C_{m_b}=C_n=0$, $1770.5\le t\le 1771.5$ s.

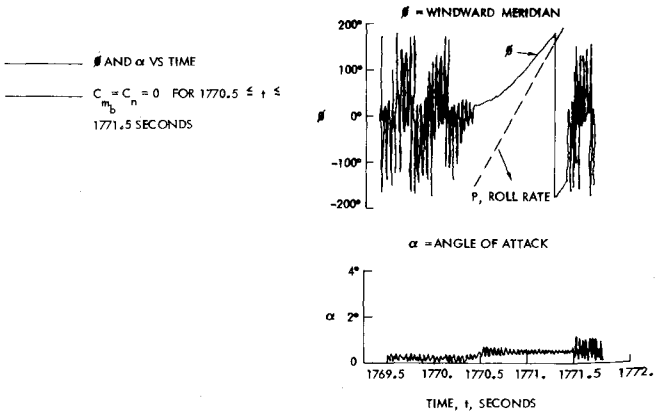

Fig. 11 6DOF simulation results ($p_0=310$ deg/s)—ϕ and α vs time—$C_{m_b}=C_n=0$, $1770.5\le t\le 1771.5$ s.

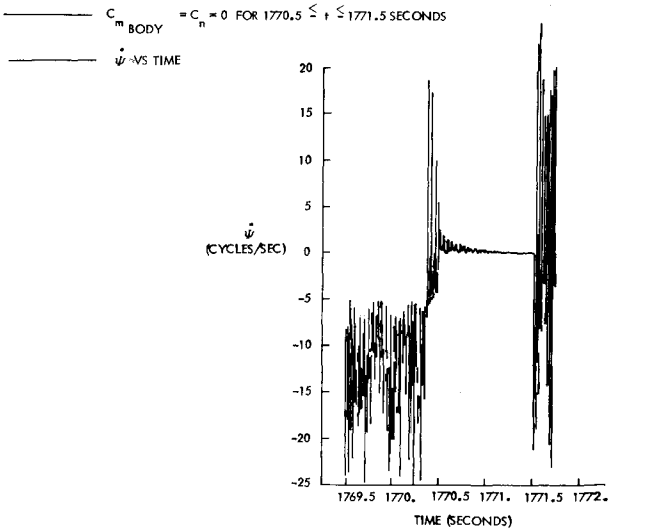

Fig. 12 6DOF simulation results ($p_0=-310$ deg/s)—$\dot{\psi}$ vs time —$C_{m_{\text{body}}}=C_n=0$ for $1770.5\le t\le 1771.5$ s.

¶The correlation between trajectory bending and the direction of spin rate cannot be explained by the effect of Yaw of Repose (Ref. 9) which would give an incorrect direction to RV dispersion.

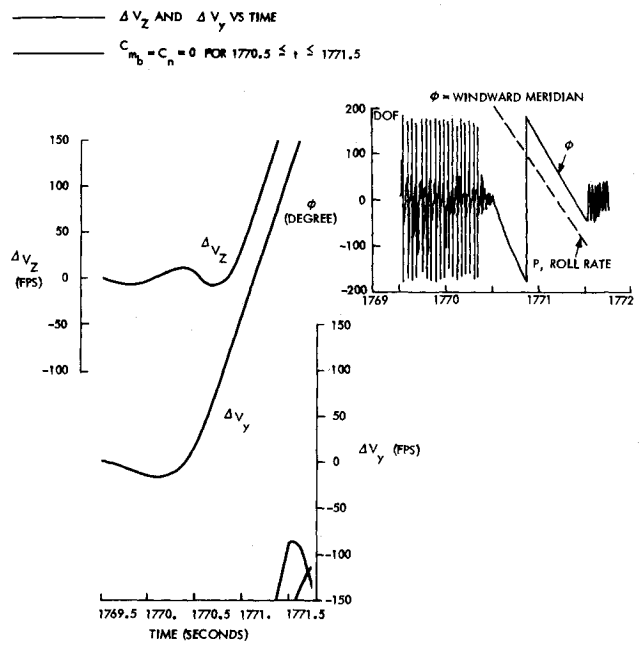

Fig. 13 6DOF simulation results ($p_0 = -310$ deg/s)—ΔV_Z and ΔV_y vs time—$C_{m_b} = C_n = 0$ for $1770.5 \le t \le 1771.5$ s.

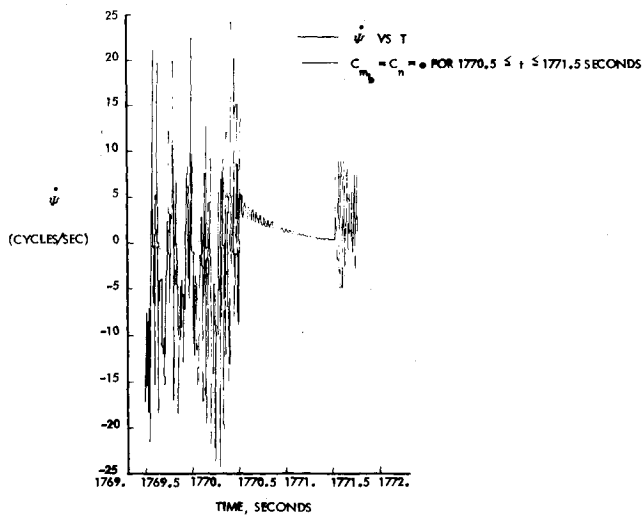

Fig. 14 6DOF simulation results ($p_0 = 930.6$ deg/s)—$\dot{\psi}$ vs time —$C_{m_b} = C_n = 0$ for $1770.5 \le t \le 1771.5$ s.

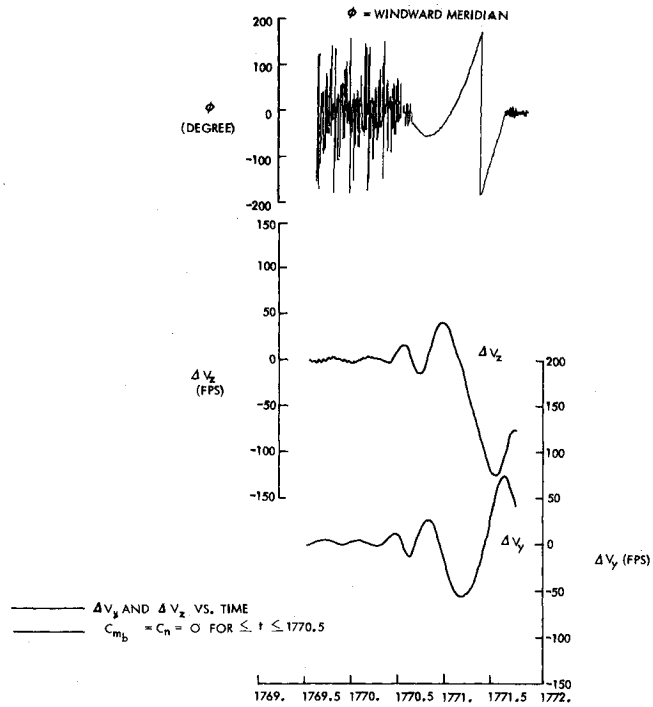

Fig. 15 6DOF simulation results ($p_0 = 930.6$ deg/s)—ΔV_y and ΔV_z vs time—$C_{m_b} = C_n = 0$ for $1770.5 \le t \le 1771.5$ s.

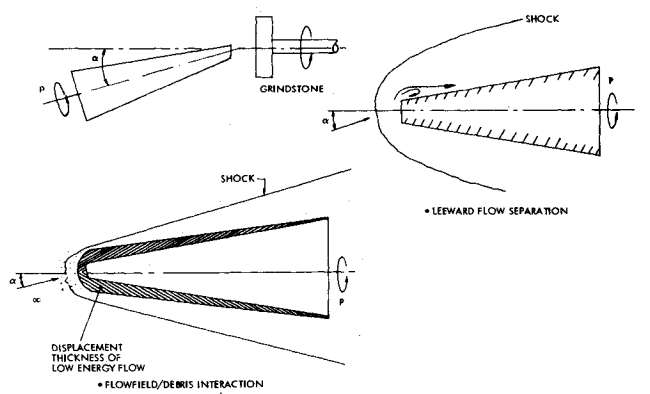

Fig. 16 Postulated physical mechanism for wind-fixed disturbance.

debris particular can permeate the front of the bow shock and reach the freestream. The resulting vortical flows are complicated and can evolve into unsteady pulsating flows.[16] Consequently, this type of two-phase flow may strongly affect RV aerodynamics (e.g., $C_{m_\alpha} \ge 0$).

The Disappearance of $C_{m_{body}}$ Coupled with the Advent of Wind-Fixed Trim Moment

It is demonstrated here with 6DOF that the precession rate would exponentially decrease to, and remain at, a near-zero value with a sudden disappearance of $C_{m_{body}}$ coupled with the advent of a wind-fixed trim moment in high q_∞ environments. Several possible mechanisms are postulated for the shift from body-fixed to wind-fixed trim moments. For instance, when an RV suddenly encounters a severely erosive environment, the nose tip recession rate can be so large that the ablation is similar to a "grindstone" phenomena (see Fig. 16). Consequently, the original body-fixed trim moment can stop the precession motion. The appearance of a wind-fixed moment can be induced by the debris in the shock layer, as mentioned before, or by the existence of flow separation on the leeward plane of spinning RV with a flat face nosetip (see Fig. 16). This flow separation can be caused by pressure gradients and/or asymmetric boundary layer transition.

Another mechanism that would cause the trim planes to migrate in a manner following the roll rate is postulated to be induced by a series of asymmetric nose spallation in a high pressure or an erosive environment. The ballistic range data suggests that the nose tip shape change process cannot be viewed in terms of the axial translation of a smooth, symmetric blunt configuration. Actually, it involves nose shape irregularities such as shoulder asymmetries. This continuous evolution of erosive shape irregularities is suggested as the basic mechanism responsible for the trim plane migration.[11]

Ablation-Time Lag Phenomena

Waterfall[6] proposed to use the ablation-time lag concept in explaining the appearance of out-of-plane moment on a spinning/ablating re-entry vehicle. Recently, several ground tests[7,8] where the models used a camphor heatshield were

designed to verify Waterfall's postulations. For instance, Morrison and Fiscina[7] measured out-of-plane force/moments which are 1 to 4% of the magnitude of the inplane values. With their measured C_n values as input to 6DOF simulation, Morrison et al.[7] did not find the catastrophic angle-of-attack divergence as observed on flight Black Knight[6]; instead they found that the effective aerodynamic dampings were increased. This numerical result can be explained by the following analytic result. Based on measurements of Ref. 7, it can be assumed that the yaw moment is:

$$C_n = -C' C_{m_\alpha}\theta, C_{m_\alpha} < 0, C' = \text{constant} < 0$$

The magnitude of C' is about 0.01-0.02. The basic equation [Eq. (5)] can be integrated as:

$$\dot{\psi}\theta^2 = (\dot{\psi}\theta^2)_0 \exp - (2\zeta\omega \pm |C'\omega^2/\dot{\psi}|)t \qquad (12)$$

where $\dot{\psi}$ is assumed to be a slow varying function.

Several observations can be made here. When $k_1 = |C'\omega^2/\dot{\psi}| < 2\zeta\omega$, the dynamic motion ($\theta$ envelope) is exponentially damped in a manner which is faster than the nominal simulation without the yaw moment. In other words, the out-of-plane moments act to enhance the aerodynamic damping coefficients (i.e., $C_{mq} + C_{m_{\dot{\alpha}}}$). This is what is observed in the 6DOF simulation of Morrison et al.[7] On the other hand, when $2\zeta\omega - k_1 < 0$, the missile angle-of-attack would exponentially diverge. This type of instability was observed in the Black Knight flight.[6] Obviously, Morrison and Fiscina's measurements correspond to the former case. This is the familiar Magnus phenomenon[13,14] which has been observed on artillery shells.

Since this out-of-plane moment/ablation-lag can amplify the aerodynamic dampings, it consequently increases the rate at which the precession stops. With a given wind fixed moment to sustain a trim angle, θ_p [see Eq. (11b)], a $2\zeta\omega + k_1 < 0$ can enhance the aerodynamic damping mechanism such that $\dot{\psi}$ is exponentially decreased to the zero value [see Eq. (11c) or (12)].

Summary

An investigation was made to identify the aerodynamic forcing functions which would induce the ballistic RV precession slowdown or stoppage. This, in turn, would result in a prohibitively large RV dispersion. In addition to the well-known phenomena of roll-through-zero, roll-near-zero, and angle-of-attack divergence, four forcing functions were obtained from analytical studies. These functions were used in 6DOF simulations and the numerical results essentially confirmed the simple closed form solutions. Of the four, the sudden disappearance of a body-fixed disturbance coupled with the introduction of a wind-fixed trim moment in a high q_∞ environment, or the situation where Magnus-type yaw moment exists, are of particular interest and significant. Furthermore, it was found that the initial roll rates before the advent of anomalous forcing function can be important in determining the magnitude as well as the directions of the trajectory deflections. Additionally, the physical mechanisms and circumstances (e.g., boundary layer transition or weather erosion, etc.) that can cause these forcing functions are delineated.

Finally, it should be emphasized that the mechanisms of inducing the forcing functions discussed in the paper are of speculative nature. Flight measurements and/or ground tests are required to verify their validity and existences.

References

[1] Platus, D. H., "Dispersion of Spinning Missiles Due to Lift Non-Averaging," *AIAA Journal*, Vol. 15, July 1977, pp. 909-915.

[2] Crenshaw, J. P., "Effect of Lift with Roll Rate Variation on Reentry Vehicle Impact," *Journal of Spacecraft and Rockets*, Vol 8, May 1971, pp. 483-488.

[3] Crenshaw, J. P., "Effect of Lift Variation on the Impact of a Rolling Reentry Vehicle," *Journal of Spacecraft and Rockets*, Vol. 9, April 1972, pp. 284-286.

[4] Murphy, C. H. and Bradley, J. W., "Jump Due to Aerodynamic Asymmetry of a Missile with Varying Roll Rate," Ballistic Research Laboratories, Aberdeen Proving Ground, MD, BRL-1077, May 1959.

[5] Hodapp, A. E., and Clark, E. L., Jr., "A Technique for Determining Approximate Roll Rate History for Ballistic Reentry Vehicles Having Mass, Inertia and Aerodynamic Asymmetries," Sandia Laboratories Report, SC-RR-69-804, Sept. 1970.

[6] Waterfall, A. P., "Effect of Ablation on the Dynamics of Spinning Reentry Vehicles," *Journal of Spacecraft and Rockets*, Vol. 6, Sept. 1969, pp. 1038-1044.

[7] Morrison, A. M., and Fiscina, C., "The Aerodynamic Simulation of a Reentry Configuration at High Angle-of-Attack with Spin and Mass Addition," AIAA Paper 82-0190, 11 Jan. 1982, Orlando, Fla. Also see Morrison, A. M., et al., "High Altitude High Angle-of-Attack Reentry Vehicle Dynamics," AIAA Paper 82-1306, AIAA 9th Atmospheric Flight Mechanics Conference, July 1982.

[8] Hull, L. D., French, N. J., and Chrusciel, G. T., "Reentry Vehicle Trim Resulting from Ablation Coupled with Motion," AIAA Paper No. 81-1862, Atmospheric Flight Mechanics Meeting, Aug. 1981.

[9] Vaughn, H. R. and Wilson, G. G., "Effect of Yaw of Repose on Ballistic Match of Similar Projectiles," *AIAA Journal*, Vol 9, June 1971, pp. 1808-1210.

[10] Siegleman, D., and Hines, R., "An Approximate Analysis of Roll/Trim Dispersion," *Journal of Spacecraft and Rockets*, Vol 16, Jan.-Feb. 1979, pp. 15-19.

[11] Thyson, N., Siegleman, D., Reeves, B., and Waldman, G., Avco Systems Division, Wilmington, Mass., private communication, July 1981.

[12] Fuess, B. F., "Impact Dispersion Due to Mass and Aerodynamic Asymmetries," *Journal of Spacecraft and Rockets*, Vol 4, Oct. 1967, pp. 1402.

[13] Platus, D. H., "Ballistic Re-entry Vehicle Flight Dynamics," *Journal of Guidance and Control*, Vol 5, Jan. 1982, p. 4.

[14] Murphy, C. H., "Symmetric Missile Dynamic Instabilities—A Survey," *Journal of Guidance and Control*, Vol 4, Sept. 1981, pp. 464-471. Also, see Murphy, C. H., "Free-Flight Motion of Symmetric Missiles," U.S. Army Ballistic Research Laboratories Report No. 1216, July 1963.

[15] Lundell, J. H., "Spallation of the Galileo Probe Heat Shield," AIAA Paper 82-0852, St. Louis, Mo., June 1982.

[16] Holden, M. S., "Studies of Transitional Flow, Unsteady Separation Phenomena and Particle Induced Heating Augmentation on Ablated Nosetip," AIAA Paper 76-320, July 1976.